Detailed QCD analysis of the photon structure function

M. Glück, K. Grassie, and E. Reya
Institut für Physik, Universität Dortmund, 4600 Dortmund 50, West Germany
(Received 15 November 1983; revised manuscript received 11 May 1984)

The effects of nonasymptotic terms in the photon structure function $F_2^\gamma(x,Q^2)$ predicted by QCD are studied directly in x space in leading and subleading order. The full (regular) solution including the hadronic nonasymptotic (${Q_0}^2$-dependent input) terms is shown to be free from the unphysical singularities of the asymptotic solution and is furthermore positive definite for suitable chosen boundary conditions (at $Q^2={Q_0}^2$) and in the physically relevant x region ($W \gtrsim 2$ GeV). The implications of the nonasymptotic solution and of their perturbatively uncalculable boundary conditions for the determination of Λ and for the predictive power of purely perturbative QCD in the determination of $F_2^\gamma(x,Q^2)$ are critically analyzed. Furthermore, taking carefully into account charm production, detailed predictions are given for present and future (unfolded) data. Similarly to the case of deep-inelastic lepton-nucleon scattering, the (nonperturbative) photonic input parton distributions at $Q^2={Q_0}^2$ are different for leading- and higher-order calculations. This implies that the differences between leading- and higher-order predictions for $F_2^\gamma(x,Q^2)$ are too small to be distinguished by present experiments. The only clean test of QCD, independent of the hadronic input, can be achieved by observing an increase of $F_2^\gamma(x,Q^2)$ with $\ln Q^2$ for fixed values of x.

I. INTRODUCTION

The comparison of the QCD predictions for the photon structure function $F_2^\gamma(x,Q^2)$ with experiment is now fully under way as improved data over a wide range of Q^2 become available. In these comparisons it was customary up to now to take for the theoretical QCD predictions just the *asymptotic* leading-order or higher-order results of Witten[1] or of Bardeen and Buras,[2] respectively.

In a previous publication[3] we pointed out the reasons for the inadequacy of the asymptotic[1,2] formulas. This inadequacy is not only due to the relatively low present values of Q^2 but mainly due to the mathematical deficiencies of the asymptotic formulas. The difficulties encountered, for example, by Duke and Owens[4] in the small-x region were realized by Bardeen[5] to be intimately related to the nonasymptotic and previously neglected hadronic components of the photon. The relation to the boundary conditions of the evolution equations for the quark and gluon distributions in the (real) photon was finally *explicitly* recognized and formulated in Ref. 3.

In this article we present detailed numerical results using the formulas developed in Ref. 3. We start, in Sec. II, by comparing the asymptotic and the full solutions in leading order and demonstrate the importance of the nonasymptotic terms at the presently available values of Q^2. In Sec. III, devoted to the higher-order QCD predictions, we first demonstrate the *positivity* of the full solution as contrasted with the asymptotic results of Duke and Owens[4] in the small-x region. We thus confirm the anticipations articulated in Ref. 3 and demonstrate the crucial *theoretical* importance of a correct treatment of the boundary conditions. Moreover, since the input parton distributions (at $Q^2={Q_0}^2$) beyond the leading order are different from the (measurable) ones in leading order, the full leading- and higher-order QCD predictions for $F_2^\gamma(x,Q^2)$ are practically indistinguishable by present experiments. We present detailed predictions for $F_2^\gamma(x,Q^2)$ with special emphasis on treating charm production in the threshold region by the well-known lowest-order associated (Bethe-Heitler box) process $\gamma^*(Q^2)\gamma\to c\bar{c}$. Furthermore, a few detailed comparisons with recent data are presented.

The implications of our results are finally discussed in Sec. IV, where, among other things, we critically discuss the reduced predictive power of perturbative QCD in the theoretical determination of $F_2^\gamma(x,Q^2)$, for presently available values of Q^2, due to the unknown hadronic quark and gluon components of the photon.

II. LEADING-ORDER RESULTS

In contrast to the deep-inelastic lepton-nucleon case, the parton distributions in the photon $q_i^\gamma(x,Q^2)$ satisfy *inhomogeneous* evolution equations[6,7] which in leading order (LO) read

$$\frac{dq_i^\gamma(x,Q^2)}{d\ln Q^2} = \frac{\alpha}{2\pi}k_i^{(0)}(x)+\frac{\alpha_s(Q^2)}{2\pi}\int_x^1\frac{dy}{y}P_i^{(0)}\left[\frac{x}{y}\right]q_i^\gamma(y,Q^2)\,, \tag{2.1}$$

where $\alpha\simeq\frac{1}{137}$,

$$\alpha_s(Q^2)=4\pi/(\beta_0\ln Q^2/\Lambda^2)$$

with $\beta_0=11-2f/3$, f being the number of flavors, and the $k_i^{(0)}$'s are the (inhomogeneous) Born terms and refer to the $\gamma\to$ quark and $\gamma\to$ gluon splitting functions. This equation is straightforward for the nonsinglet case $i=\mathrm{NS}$ where

$$k_{\rm NS}^{(0)}=3f(\langle e^4\rangle-\langle e^2\rangle^2)2[x^2+(1-x)^2],\quad P_{\rm NS}^{(0)}\equiv P_{qq}^{(0)}\ , \tag{2.2}$$

with

$$\langle e^k\rangle \equiv \frac{1}{f}\sum_f e_q^k$$

and $P_{qq}^{(0)}$ is the standard Altarelli-Parisi splitting function. In the singlet case $i=\mathrm{S}$, however, Eq. (2.1) becomes a (coupled) matrix equation with

$$q_{\rm S}^{\gamma}\equiv\begin{bmatrix}\Sigma^\gamma\\ G^\gamma\end{bmatrix},\quad k_{\rm S}^{(0)}\equiv\begin{bmatrix}k_q^{(0)}\\ 0\end{bmatrix},$$
$$P_{\rm S}^{(0)}\equiv\begin{bmatrix}P_{qq}^{(0)} & P_{qg}^{(0)}\\ P_{gq}^{(0)} & P_{gg}^{(0)}\end{bmatrix}, \tag{2.3}$$

where

$$k_q^{(0)}(x)=3f\langle e^2\rangle 2[x^2+(1-x)^2]\ .$$

From the solutions of Eq. (2.1) one obtains the measured photon structure function $F_2^\gamma(x,Q^2)$ by

$$\frac{1}{x}F_2^\gamma(x,Q^2)=q_{\rm NS}^\gamma(x,Q^2)+\langle e^2\rangle\Sigma^\gamma(x,Q^2)\ . \tag{2.4}$$

To obtain the most general solution of Eq. (2.1) it is clear that one needs, as in the deep-inelastic lepton-nucleon case, input distributions $q_i^\gamma(x,Q_0{}^2)$ at a given value of $Q^2=Q_0{}^2$ which include the nonpointlike hadronic piece of the photon and, strictly speaking, have to be extracted from experiment. Since these nonpointlike contributions in the solution of (2.1) are formally suppressed like

$$[\alpha_s(Q^2)/\alpha_s(Q_0{}^2)]^{-2P^{(0)}/\beta_0}\ ,$$

it has become customary to neglect these terms and to keep only those terms which are proportional to $\ln Q^2/\Lambda^2$, which constitute the so-called asymptotic or pointlike solution. This latter solution is unique to the extent that it does not depend on the unknown input quantities ("boundary conditions") $Q_0{}^2$ and $q_i^\gamma(x,Q_0{}^2)$. The hadronic nonpointlike pieces are then estimated using vector-meson-dominance (VMD) arguments and are added to the "unique" pointlike solution. As we shall discuss later such a separation of pointlike and nonpointlike contributions to F_2^γ is not only incorrect from a mathematical as well as physical point of view but we shall also see that the input boundary conditions at $Q_0{}^2$ are by far not negligible at currently available values of Q^2.

Nevertheless, in order to demonstrate more clearly the differences between the general solution of Eq. (2.1) and the asymptotic solution so far used, we briefly consider the latter one first. The *asymptotic* pointlike solution of the evolution equations (2.1) is of the general form[6]

$$q_i^\gamma(x,Q^2)=\frac{4\pi}{\alpha_s(Q^2)}a_i(x) \tag{2.5}$$

which, when inserted into Eq. (2.1), yields a simple integral equation for $a_i(x)$:

$$a_i(x)=\frac{\alpha}{2\pi\beta_0}k_i^{(0)}(x)+\frac{2}{\beta_0}\int_x^1\frac{dy}{y}P_i^{(0)}\left[\frac{x}{y}\right]a_i(y)\ , \tag{2.6}$$

where

$$a_{\rm S}=\begin{bmatrix}a_\Sigma\\ a_G\end{bmatrix}.$$

These equations are easily solved by iteration[8] and the well-known results[6] are shown by the short-dashed curves in Figs. 1 and 2 for $f=4$ and $f=3$ flavors, respectively.

It should be noted in passing that sometimes the x-dependent predictions are extracted from the QCD predictions for Mellin moments, defined by

$$q_i^\gamma(n,Q^2)\equiv\int_0^1 dx\, x^{n-1}q_i^\gamma(x,Q^2)\ , \tag{2.7}$$

which are fitted by using some *ad hoc* x-dependent ansatz for $F_2^\gamma(x,Q^2)$ where supplementary considerations must be invoked to determine the end-point behavior. In Fig. 1 we compare the results obtained in this way[2,4] (crossed curves) and one sees that they differ appreciably from the exact solutions obtained directly in Bjorken-x space.[6] Because of the simple analytic structure of the LO QCD mo-

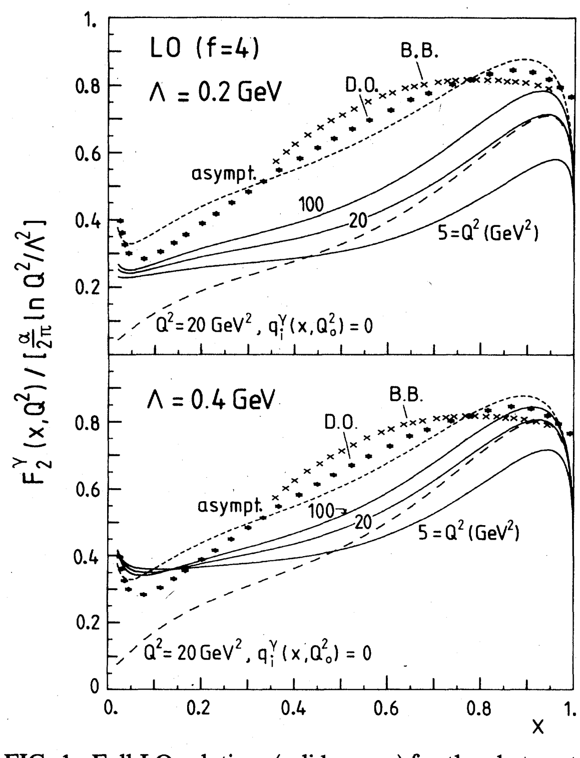

FIG. 1. Full LO solutions (solid curves) for the photon structure functions for $f=4$ flavors and for two different values for Λ using the VMD input of Eq. (2.9) at $Q_0{}^2=1$ GeV^2. The long-dashed curves show the effect of the boundary conditions at $Q^2=20$ GeV^2 for vanishing input distributions [cf. Eq. (2.11)]. The exact asymptotic solutions, Eqs. (2.5) and (2.6), are shown by the short-dashed curves, which are of course the same in the two pictures, and compared with the appropriate results (crossed curves) of Ref. 2 (B.B.) and Ref. 4 (D.O.) obtained by fitting some x-dependent ansatz to QCD moments.

ments, one can also perform a direct numerical Mellin inversion[1] and the results agree of course with those obtained by solving the evolution equations directly in x space (short-dashed curves in Figs. 1 and 2). In higher orders, however, such a direct numerical Mellin inversion is not possible anymore because the singularity structure of the predicted moments is too complicated in n space; therefore one is either forced to use the indirect and approximate fitting method[2,4] described above or, more appropriately, to solve the evolution equations *directly* in Bjorken-x space which will be done in Sec. III.

As already emphasized the separation of the perturbative asymptotic pointlike and the hadronic nonpointlike (VMD) contribution to F_2^γ, i.e., $F_2^\gamma=$ pointlike + VMD, where VMD is nonsingular, is incorrect.[3,9,10] The intuitive reason for this has been recently reemphasized by Frazer[9] who pointed out that the infrared singularities of the ladder diagram [Fig. 3(a)], which makes up the asymptotic pointlike result,[1,2] must be canceled by infrared singularities of the diagrams in Figs. 3(b) and 3(c). The diagram of Fig. 3(b), however, is of the type associated with VMD, i.e., with $q\bar{q}$ bound states. Therefore the VMD terms *must* contain singularities to cancel the ones of the pointlike terms. Thus, the usual prescription $F_2^\gamma=$ pointlike + VMD, where VMD is *regular*, is wrong. Mathematically such a separation results in difficulties concerning singularities at $x=0$ in the asymptotic pointlike terms usually considered: The leading-order Witten result[1] for $F_2^\gamma(x,Q^2)$ diverges as $x^{-0.5964}$ due to the rightmost pole in the moment $\Sigma^\gamma(n,Q^2)$ at $n=1.5964$ for $f=4$ flavors. In the next order one finds a divergence like x^{-1} due to a pole at $n=2$ which would result in (unphysical) negative structure functions[4] at small values of x. It has been speculated by Rossi[10] that these divergences might become even worse if one goes to even higher orders and could extend over the entire region of x. All these difficulties with mathematically ill-defined asymptotic terms are eliminated if one considers, as one has to, the *general* solutions of the evolution equations (2.1), i.e., by taking into account the hadronic input distributions at Q_0^2 (boundary conditions) from the very beginning.

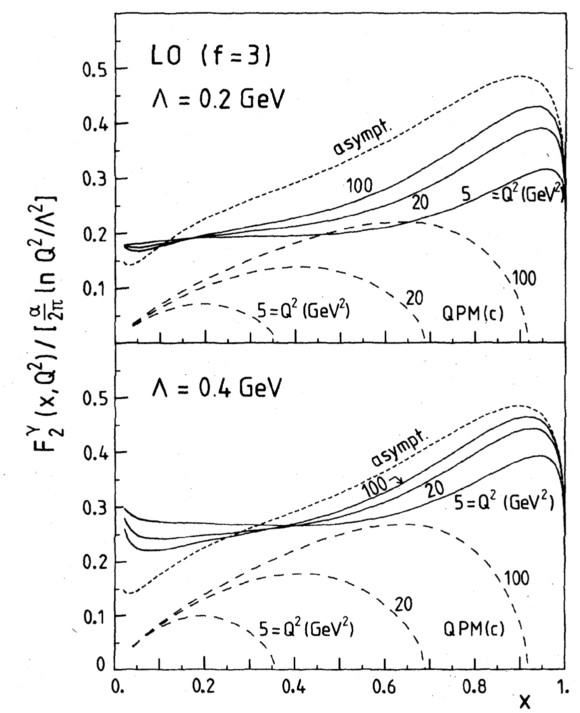

FIG. 2. Full LO solutions (solid curves) for the photon structure functions for $f=3$ flavors and for two different values of Λ using the VMD input of Eq. (2.9) at $Q_0^2=1$ GeV^2. The long-dashed curves are the QPM predictions for charm production according to Eq. (2.13) using $m_c=1.5$ GeV.

In order to obtain the *general* solutions of Eq. (2.1) one clearly needs the hadronic input distributions $q_i^\gamma(x,Q_0^2)$ at some initial $Q^2=Q_0^2$ (boundary conditions). Strictly speaking these nonperturbative quantities have to be determined experimentally, as in the case of deep-inelastic lepton-nucleon scattering. Present two-photon measurements, however, do not suffice to delineate the three input quantities $q_{NS}^\gamma(x,Q_0^2)$, $\Sigma^\gamma(x,Q_0^2)$, and $G^\gamma(x,Q_0^2)$. We therefore assume, as is commonly done, that this input can be estimated on grounds of VMD ideas[7] although one should keep in mind that VMD probably underestimates the "real" hadronic input at Q_0^2 especially at large values of x. Typically $Q_0^2\simeq 1$ GeV^2 where VMD is in good agreement with the measured total $\gamma\gamma$ cross section, but for $Q^2>Q_0^2\simeq 1$ GeV^2 there is a clear deviation[11] from the VMD expectations which points toward the onset of the pointlike partonic contribution. The VMD contribution to the photon structure function is dominantly given by,[7,12] at a given value of Q^2,

$$F_{2,\mathrm{VMD}}^\gamma(x,Q^2)\simeq\frac{4\pi\alpha}{f_\rho^{\,2}}\sum_i e_i^{\,2}xq_i^{\rho^0}(x,Q^2) \tag{2.8}$$

with $f_\rho^{\,2}/4\pi\simeq 2$ and where one assumes $q_i^{\rho^0}(x,Q^2)$ to be the same as those for π^0, i.e., $q^{\rho^0}=q^{\pi^0}=\frac{1}{2}(q^{\pi^+}+q^{\pi^-})$, and their evolutions with Q^2 are well known[13] according to the standard (homogeneous) Altarelli-Parisi equations. Writing Eq. (2.8) in our nonsinglet and singlet basis we finally get

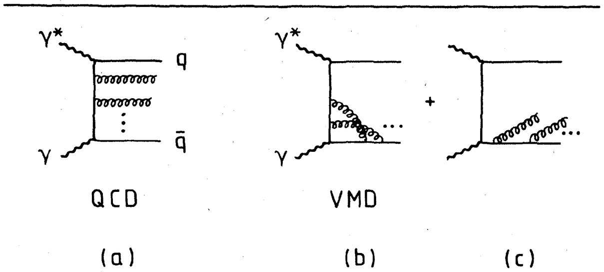

FIG. 3. Diagrams leading to infrared singularities: (a) in the pointlike asymptotic solutions (Refs. 1 and 2) and (b) and (c) in the hadronic input distributions. Diagram (b) simulates the $q\bar{q}$ bound vector state (VMD).

$$q_{\mathrm{NS,VMD}}^{\gamma}(x,Q^2)=\frac{4\pi\alpha}{f_\rho^{\,2}}\times\begin{cases}\frac{1}{9}v^{\pi} & (f=3),\\ -\frac{1}{3}\xi^{\pi} & (f=4),\end{cases}$$

$$\Sigma_{\mathrm{VMD}}^{\gamma}(x,Q^2)=\frac{4\pi\alpha}{f_\rho^{\,2}}(2v^{\pi}+6\xi^{\pi}) , \qquad (2.9)$$

$$G_{\mathrm{VMD}}^{\gamma}(x,Q^2)=\frac{4\pi\alpha}{f_\rho^{\,2}}G^{\pi} ,$$

where the pionic parton distributions are taken from Ref. 13 using the same valence and sea decompositions, namely,

$$u^{\pi^+}=\bar{d}^{\,\pi^+}=\bar{u}^{\,\pi^-}=d^{\pi^-}=v^{\pi}+\xi^{\pi} ,$$
$$\bar{u}^{\,\pi^+}=d^{\pi^+}=u^{\pi^-}=\bar{d}^{\,\pi^-}\simeq s^{\pi^{\pm}}=\bar{s}^{\pi^{\pm}}\equiv\xi^{\pi} . \qquad (2.10)$$

All these results are adopted at $Q^2=Q_0^{\,2}\simeq 1$ GeV^2 for our hadronic input. The small (intrinsic) photonic charm distributions $c^{\gamma},\bar{c}^{\gamma}$ have been neglected in Eq. (2.9)—charm production in the threshold region is expected to be entirely described by the lowest-order Bethe-Heitler process $\gamma^*\gamma\to c\bar{c}$.

It should, however, be emphasized that in order to obtain a better agreement between theory and experiment one might be forced to use initial values for $q_i^{\gamma}(x,Q_0^{\,2})$ *other* than suggested by VMD. This is so because it is by far not obvious that there exists any $Q_0^{\,2}$ at all, even in the $\lesssim 1$-GeV^2 region, where the photon is entirely prescribed by the VMD ansatz.

The final results for $f=4$ flavors are shown in Fig. 1 by the solid curves for various values of Q^2 and two choices for Λ. It is clear that at presently attainable values of $Q^2(\lesssim 100$ GeV$^2)$ the effects of the hadronic boundary conditions at $Q_0^{\,2}=1$ GeV^2 are *not* negligible[14] throughout the *whole* x region and therefore the asymptotic solutions (short-dashed curves) should *not* be used for comparison with present data. To illustrate the dependence of our predictions on the chosen (VMD) input $q_i^{\gamma}(x,Q_0^{\,2})$ at $Q_0^{\,2}=1$ GeV^2, we also show the results for $q_i^{\gamma}(x,Q_0^{\,2})=0$ by the long-dashed curves (corresponding to $Q^2=20$ GeV^2): As one can see the positive spikes proportional to $x^{-0.5964}$ at small x in the asymptotic solutions disappear due to taking into account the boundary conditions at $Q_0^{\,2}$. The reason for this becomes immediately transparent if one writes the general full solution of Eq. (2.1) for moments,[3] defined by Eq. (2.7),

$$q_i^{\gamma}(n,Q^2)=\frac{4\pi}{\alpha_s(Q^2)}\left[1-\left[\frac{\alpha_s(Q^2)}{\alpha_s(Q_0^{\,2})}\right]^{1-2P_i^{(0)}(n)/\beta_0}\right]a_i(n)+\left[\frac{\alpha_s(Q^2)}{\alpha_s(Q_0^{\,2})}\right]^{-2P_i^{(0)}(n)/\beta_0}q_i^{\gamma}(n,Q_0^{\,2}) \qquad (2.11)$$

to be compared with the asymptotic solution (2.5). Thus artificial poles in a_i are regularized by the vanishing of the square bracket in Eq. (2.11), i.e.,

$$\lim_{\epsilon\to 0}(1-\alpha^{\epsilon})\frac{1}{\epsilon}=-\ln\alpha , \qquad (2.12)$$

which explicitly demonstrates how indispensable the full solution is for obtaining physically and mathematically well-behaved predictions for the photon structure function—this will be of vital importance when higher orders are included. Furthermore, it is clear from Eq. (2.11) that this regularization is independent of the detailed form of the input $q_i^{\gamma}(x,Q_0^{\,2})$ and depends only on the chosen value of $Q_0^{\,2}$ via $\alpha_s(Q_0^{\,2})$. Finally it should be stressed that all the perturbative predictions in Fig. 1, as well as all forthcoming results, should be taken seriously only for $W\gtrsim 2$ GeV and $Q^2\gtrsim 1$ GeV^2 where $W^2=Q^2(1/x-1)$.

For a realistic comparison of LO predictions with (most) present experiments (where $Q^2\lesssim 50$ GeV^2) one should *not* use the $f=4$ results of Fig. 1, since in the charm-threshold region where $Q^2 \ggg 4m_c^{\,2}$ charm production must not be treated as the standard light quarks (u,d,s) but instead must be accounted for by the well-known lowest-order quark-parton-model (QPM) cross section for the (Bethe-Heitler) process $\gamma^*(Q^2)\gamma\to c\bar{c}$, similar to the case of deep-inelastic lepton-hadron scattering,[15]

$$\frac{1}{x}F_{2,c}^{\gamma}(x,Q^2)=3\left[\frac{4}{9}\right]^2\frac{\alpha}{\pi}\left\{\beta\left[8x(1-x)-1-\frac{4m_c^{\,2}}{Q^2}x(1-x)\right]+\left[x^2+(1-x)^2+\frac{4m_c^{\,2}}{Q^2}x(1-3x)-\frac{8m_c^{\,4}}{Q^4}x^2\right]\ln\frac{1+\beta}{1-\beta}\right\} , \qquad (2.13)$$

where

$$\beta^2=1-4m_c^{\,2}x/(1-x)Q^2 .$$

For $\beta^2<0$, i.e., $W<2m_c$, $F_{2,c}^{\gamma}\equiv 0$. We use throughout $m_c=1.5$ GeV. A few predictions due to Eq. (2.13) are shown by the long-dashed curves in Fig. 2 which have to be *added* to the $f=3$ flavor (u,d,s) results shown by the solid curves. Only for $Q^2\gtrsim 100$ GeV^2 one can use the fully renormalization-group-improved results for $f=4$ light quarks as shown, for example, in Fig. 1.

As we shall see these LO predictions are in disagreement with present preliminary data, i.e., they fall *below* present measurements. This might indicate that the input at $Q^2=Q_0^{\,2}\simeq 1$ GeV^2 is not simply given by VMD, Eq. (2.9), but perhaps by VMD *and* the naive QPM (box) cross section—a combination which provides already a reasonable description[11,16] of the data at a given value of Q^2. The various LO predictions will be given in comparison with the respective higher-order ones to be discussed next.

III. HIGHER-ORDER CONTRIBUTIONS

Generalizing the LO evolution equations (2.1) to the next-to-leading order one obtains[3]

$$\frac{dq_i^\gamma(x,Q^2)}{d\ln Q^2}=\frac{\alpha}{2\pi}\left[k_i^{(0)}(x)+\frac{\alpha_s(Q^2)}{2\pi}k_i^{(1)}(x)\right]+\frac{\alpha_s(Q^2)}{2\pi}\left[P_i^{(0)}+\frac{\alpha_s(Q^2)}{2\pi}P_i^{(1)}\right]*q_i^\gamma \tag{3.1}$$

with the convolutions defined by

$$P*q\equiv\int_x^1\frac{dy}{y}P\left[\frac{x}{y}\right]q(y,Q^2) \tag{3.2}$$

and

$$\frac{4\pi}{\alpha_s(Q^2)}=\beta_0\ln\frac{Q^2}{\Lambda^2}+\frac{\beta_1}{\beta_0}\ln\ln\frac{Q^2}{\Lambda^2}\ , \tag{3.3}$$

where $\beta_1=102-38f/3$ and Λ as well as all higher-order (HO) results throughout this paper refer to the modified minimal-subtraction ($\overline{\text{MS}}$) scheme. Explicit analytic expressions for the HO photon-parton splitting functions $k_{i=\text{NS}}^{(1)}(x)$ and[17]

$$k_{\text{S}}^{(1)}\equiv\begin{bmatrix}k_q^{(1)}\\ k_G^{(1)}\end{bmatrix}$$

are given in Ref. 3 where also simple analytic expressions[18] for $P_{\text{NS}}^{(1)}(x)$ and $P_{\text{S}}^{(1)}(x)$, the latter matrix being defined similarly to $P_{\text{S}}^{(0)}$ in Eq. (2.3), can be found. In contrast to Eq. (2.4), the measured photon structure function is now obtained from

$$\frac{1}{x}F_2^\gamma(x,Q^2)=q_{\text{NS}}^\gamma(x,Q^2)+\frac{\alpha_s(Q^2)}{4\pi}B_q*q_{\text{NS}}^\gamma+\langle e^2\rangle\left[\Sigma^\gamma(x,Q^2)+\frac{\alpha_s(Q^2)}{4\pi}(B_q*\Sigma^\gamma+B_G*G^\gamma)\right]+3f\langle e^4\rangle\frac{\alpha}{4\pi}B_\gamma(x) \tag{3.4}$$

with the convolutions defined in Eq. (3.2) and the various Wilson coefficients $B_j(x)$ are summarized in Ref. 3. It should be emphasized that, in contrast to the LO case, the photonic parton distributions $q_i^\gamma(x,Q^2)$ by themselves have *no* direct physical meaning; only the combination (3.4) with Wilson coefficient represents, to a given order in α_s, a measurable quantity which is independent of the renormalization convention adopted,[19] apart of course from the prescription dependence inherent in defining α_s. Therefore the boundary conditions at $Q_0{}^2$, i.e., the (unknown) input distributions $q_i^\gamma(x,Q_0{}^2)$, required for the full solution of Eq. (3.1), can in general be *different* from the ones for LO calculations. The situation is here identical to the well-known case of deep-inelastic lepton-nucleon scattering where the unphysical input distributions for the HO predictions are different from the physical LO ones.[20–22]

A. Asymptotic solution

The asymptotic pointlike HO "solution" is the one[2] where only terms proportional to $\alpha_s{}^{-1}(Q^2)$ and "constant" terms independent of α_s are kept, whereas all other pieces appearing in the general full solution of Eq. (3.1) are neglected. Following Eq. (2.5) it can be obtained from the ansatz

$$q_i^\gamma(x,Q^2)=\frac{4\pi}{\alpha_s(Q^2)}a_i(x)+b_i(x) \tag{3.5}$$

which, when inserted into Eq. (3.1), yields the same integral equation (2.6) for $a_i(x)$ whereas $b_{i=\text{NS,S}}(x)$ satisfies[3]

$$-P_i^{(0)}*b_i=\frac{\alpha}{2\pi}\left[k^{(1)}(x)-\frac{\beta_1}{2\beta_0}k^{(0)}(x)\right]+2\left[P_i^{(1)}-\frac{\beta_1}{2\beta_0}P_i^{(0)}\right]*a_i\ , \tag{3.6}$$

where

$$b_{\text{S}}\equiv\begin{bmatrix}b_\Sigma\\ b_G\end{bmatrix}.$$

Again Eq. (3.6) is easily solved numerically by iteration.[23] The final expression for the photon structure function then follows from inserting $q_i^\gamma(x,Q^2)$ in Eq. (3.5) into Eq. (3.4):

$$\frac{1}{x}F_2^\gamma(x,Q^2)=\frac{4\pi}{\alpha_s(Q^2)}[a_{\text{NS}}(x)+\langle e^2\rangle a_\Sigma(x)]+b_{\text{NS}}(x)+\langle e^2\rangle b_\Sigma(x)+B_q*a_{\text{NS}}+\langle e^2\rangle(B_q*a_\Sigma+B_G*a_G)+3f\langle e^4\rangle\frac{\alpha}{4\pi}B_\gamma(x)+O(\alpha_s)\ , \tag{3.7}$$

where the $O(\alpha_s)$ terms arising through the combination of Eqs. (3.4) and (3.5) should, strictly speaking, be omitted here since their complete inclusion affords a treatment of the evolution equations (3.1) beyond the order here considered.

Equation (3.6) for $b_i(x)$ is entirely new. It allows one to solve for b_i *directly* in Bjorken-x space. We show for illustration in Fig. 4 the explicit results for $b_i(x)$ for $f=4$ flavors together with the well-known[6] previously obtained LO results for $a_i(x)$ which appear in Eq. (3.6) for $b_i(x)$.

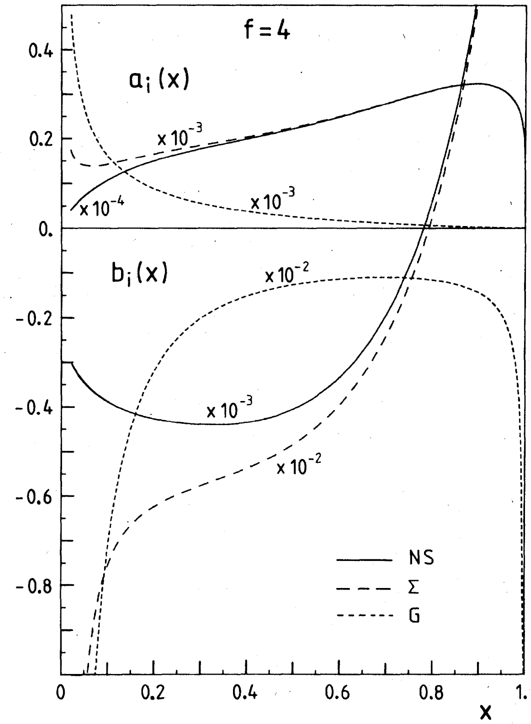

FIG. 4. Solutions of Eq. (2.6) for $a_i(x)$ and Eq. (3.6) for $b_i(x)$ for $f=4$ flavors. The final results are obtained by multiplying the curves by the indicated powers of 10.

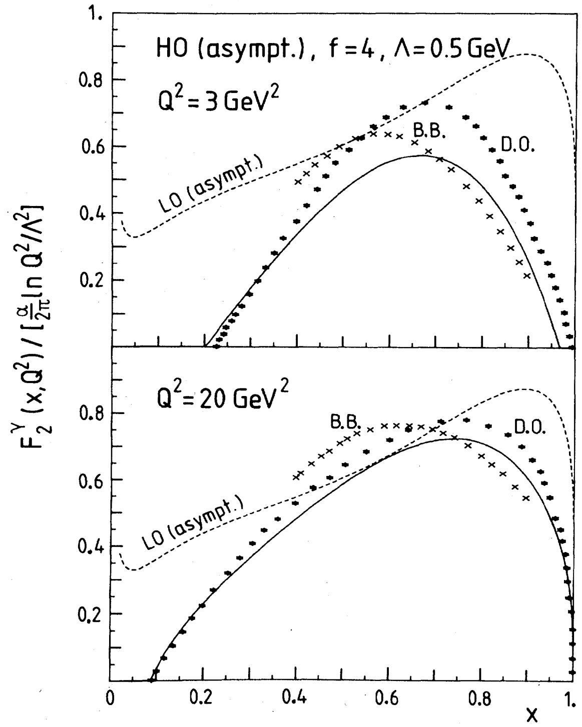

FIG. 5. Asymptotic HO solutions (solid curves) for the photon structure function given by Eq. (3.7) for $f=4$ flavors and $\Lambda\equiv\Lambda_{\overline{\rm MS}}=0.5$ GeV. Our exact results are compared with the approximate ones (crossed curves) of Ref. 2 (B.B.) and Ref. 4 (D.O.) obtained by fitting some x-dependent ansatz to QCD moments.

As one can see the two singlet quantities $b_\Sigma(x)$ and $b_G(x)$, shown by the dashed curves in Fig. 4, become strongly *negative* for $x\rightarrow 0$, diverging like $-x^{-2}$, in contrast to the small positive spikes of $a_\Sigma(x)$ and $a_G(x)$ proportional to $x^{-1.5964}$ as discussed in the previous section. The reason for this can be readily understood from Eq. (3.6):[3] Taking the nth Mellin moment, defined by Eq. (2.7), one observes that $b_s(n)$ is proportional to the inverse of the singlet anomalous dimension matrix $P_S^{(0)}(n)^{-1}$ defined in Eq. (2.3); thus $b_S(n)$ develops a pole at $n=2$ with *negative* residue due to the vanishing of one eigenvalue of $P_S^{(0)}(n=2)$ reflecting energy-momentum conservation. This $n=2$ pole implies in x space a (negative) spike proportional to x^{-2}, for small values of x, which extends to larger values of x than the weaker divergence proportional to $x^{-1.5964}$ in $a_\Sigma(x)$ and $a_G(x)$.

The fact that $b_i(x)$ is strongly negative in the small-x region causes $F_2^\gamma(x,Q^2)$ in Eq. (3.7) to become *negative*[4] for $x\lesssim 0.2$ in the presently accessible range of $Q^2(\lesssim 100$ GeV$^2)$ where the first term on the right-hand side (RHS) of Eq. (3.5) is not yet the entirely dominant one. The results for two values of Q^2 are shown in Fig. 5 by the solid curves and are compared with the ones[2,4] obtained by fitting some x-dependent ansatz for $F_2^\gamma(x,Q^2)$ to the moments predicted by QCD (crossed curves). These latter approximate results differ appreciably from our exact solutions, the differences being even larger than in the LO case (cf. Fig. 1), although the intercepts in x where F_2^γ turns negative have been surprisingly well reproduced.[4]

Clearly, negative values of the structure function $F_2^\gamma(x,Q^2)$ are unphysical and their appearance is not very surprising since they result from a mathematically ill-defined quantity, $b_S(n=2)=\infty$. Such difficulties occur, however, *only* in the asymptotic solution (3.5) which is obtained by arbitrarily truncating the general full solution of Eq. (3.1), i.e., by disregarding all input boundary conditions at $Q^2=Q_0{}^2$ which, although power suppressed in $\alpha_s(Q^2)$, are in principle *not* negligible.

B. Full regular solution

To obtain the general full solution of Eq. (3.1) one needs, as in the LO case, to specify the boundary conditions at some initial $Q^2=Q_0{}^2$, i.e., the hadronic input distributions $q_i^\gamma(x,Q_0{}^2)$. Having chosen an appropriate input, the most straightforward way to find the full solutions would be to solve Eq. (3.1) by iteration and insert the results into Eq. (3.4). In this way, however, it is impossible to avoid the convention-dependent $O(\alpha_s)$ terms[24] [their complete inclusion affords a treatment of Eq. (3.1) beyond the order here considered] which were under control in Eq. (3.7) because of the explicit ansatz (3.5) for the asymptotic solution. From this direct procedure we have found that the $O(\alpha_s)$ terms, when appropriately extracted as described below, are tolerably small only for $Q^2\gtrsim 100$ GeV^2 and for present values of Λ between 0.1 and 0.5 GeV, at least as long as one works in the $\overline{\rm MS}$ or momentum-subtraction (MOM) scheme.[24] For $Q^2 \lesssim 100$ GeV^2, however, the unwanted $O(\alpha_s)$ terms turned out to be sizable, typically 30—40%, and therefore we have chosen to work not directly with Eq. (3.1) but with a method which allows us to trace and eliminate these terms explicitly.

The simplest way to sketch the method which allows us to avoid $O(\alpha_s)$ terms explicitly is to recall the solution of Eq. (3.1) for moments, defined by Eq. (2.7). This can be written in closed form as[3]

$$q_i^\gamma(n,Q^2)=\frac{4\pi}{\alpha_s(Q^2)}\left[1-\left[\frac{\alpha_s(Q^2)}{\alpha_s(Q_0{}^2)}\right]^{1-2P_i^{(0)}(n)/\beta_0}\right]a_i(n)+\left[1-\left[\frac{\alpha_s(Q^2)}{\alpha_s(Q_0{}^2)}\right]^{-2P_i^{(0)}(n)/\beta_0}\right]b_i(n)$$
$$+\alpha_s(Q^2)^{-2P_i^{(0)}(n)/\beta_0}\left\{1-\frac{\alpha_s(Q^2)-\alpha_s(Q_0{}^2)}{\pi\beta_0}\left[P_i^{(1)}(n)-\frac{\beta_1}{2\beta_0}P_i^{(0)}(n)\right]\right\}\alpha_s(Q_0{}^2)^{2P_i^{(0)}(n)/\beta_0}q_i^\gamma(n,Q_0{}^2)$$
$$+\text{ higher orders} \tag{3.8}$$

which should be compared with the LO solution (2.11). Thus, if one inverts each term in (3.8) separately to Bjorken-x space, one can, on inserting into Eq. (3.4), omit explicitly all annoying $O(\alpha_s)$ terms. The second line in Eq. (3.8) describes nothing else but the standard QCD evolution of parton distributions and is easily obtained in x space by solving the homogeneous HO evolution equations, i.e., Eq. (3.1) with $k_i^{(0)}$ and $k_i^{(1)}$ set equal to zero. Furthermore, $a_i(x)$ and $b_i(x)$ in the first line of Eq. (3.8) are the same as in the asymptotic solution (3.5) and are the solutions of Eqs. (2.6) and (3.6), respectively. So the only problem left is to invert the most important square brackets in Eq. (3.8) which multiply a_i and b_i and which regularize any artificial poles in a_i and more importantly the $n=2$ pole in b_i according to Eq. (2.12),[25] leaving us with a perfectly finite and mathematically well-defined (positive) result. According to Eq. (3.8) we have to invert the expression

$$T_i(n,Q^2,Q_0{}^2)\equiv\left[\frac{\alpha_s(Q^2)}{\alpha_s(Q_0{}^2)}\right]^{-2P_i^{(0)}(n)/\beta_0} \tag{3.9}$$

for which one can immediately read off the following evolution equation in x space:

$$\frac{dT_i(x,Q^2,Q_0{}^2)}{d\alpha_s}=-\frac{2}{\alpha_s\beta_0}P_i^{(0)}*T_i \tag{3.10}$$

with $\alpha_s=\alpha_s(Q^2)$ given by Eq. (3.3) and the convolution is defined by Eq. (3.2). Some properties of the nonsinglet quantity $T_{i=\mathrm{NS}}(x,Q^2,Q_0{}^2)$ have been studied already a long time ago[26] whereas for $i=\mathrm{S}$, Eq. (3.10) is a matrix equation since

$$T_\mathrm{S}\equiv\begin{bmatrix}T_{qq} & T_{qg}\\ T_{gq} & T_{gg}\end{bmatrix}$$

and with $P_\mathrm{S}^{(0)}$ given in Eq. (2.3). This implies two coupled integro-differential equations for T_{qq} and T_{gq} and two coupled equations for T_{qg} and T_{gg}. All these equations are again easily solved by iteration using as initial input values[17] at $Q^2=Q_0{}^2$

$$\begin{aligned}T_\mathrm{NS}(x,Q_0{}^2,Q_0{}^2)&=T_{qq}(x,Q_0{}^2,Q_0{}^2)\\&=T_{gg}(x,Q_0{}^2,Q_0{}^2)=\delta(1-x)\,,\\T_{qg}(x,Q_0{}^2,Q_0{}^2)&=T_{gq}(x,Q_0{}^2,Q_0{}^2)=0\,.\end{aligned} \tag{3.11}$$

The final result is then obtained by inserting the Mellin inverse of Eq. (3.8) into Eq. (3.4):

$$\frac{1}{x}F_2^\gamma(x,Q^2)=\frac{4\pi}{\alpha_s(Q^2)}\left\{a_\mathrm{NS}(x)-\frac{\alpha_s(Q^2)}{\alpha_s(Q_0{}^2)}T_\mathrm{NS}*a_\mathrm{NS}+\langle e^2\rangle\left[a_\Sigma(x)-\frac{\alpha_s(Q^2)}{\alpha_s(Q_0{}^2)}(T_{qq}*a_\Sigma+T_{qg}*a_G)\right]\right\}$$
$$+b_\mathrm{NS}(x)-T_\mathrm{NS}*b_\mathrm{NS}+\langle e^2\rangle[b_\Sigma(x)-T_{qq}*b_\Sigma-T_{qg}*b_G]+B_q*\left[a_\mathrm{NS}-\frac{\alpha_s(Q^2)}{\alpha_s(Q_0{}^2)}T_\mathrm{NS}*a_\mathrm{NS}\right]$$
$$+\langle e^2\rangle\left[B_q*a_\Sigma-\frac{\alpha_s(Q^2)}{\alpha_s(Q_0{}^2)}B_q*(T_{qq}*a_\Sigma+T_{qg}*a_G)+B_G*a_G-\frac{\alpha_s(Q^2)}{\alpha_s(Q_0{}^2)}B_G*(T_{gq}*a_\Sigma+T_{gg}*a_G)\right]$$
$$+3f\langle e^4\rangle\frac{\alpha}{4\pi}B_\gamma(x)+O(\alpha_s)+q_{\mathrm{NS,had}}^\gamma(x,Q^2)+\frac{\alpha_s(Q^2)}{4\pi}B_q*q_{\mathrm{NS,had}}^\gamma$$
$$+\langle e^2\rangle\left\{\Sigma_\mathrm{had}^\gamma(x,Q^2)+\frac{\alpha_s(Q^2)}{4\pi}[B_q*\Sigma_\mathrm{had}^\gamma+B_G*G_\mathrm{had}^\gamma]\right\}, \tag{3.12}$$

where the last three terms proportional to $q_{i,\mathrm{had}}^\gamma(x,Q^2)$ refer to the hadronic input parton distributions $q_i^\gamma(x,Q_0{}^2)$ evolved according to the standard homogeneous HO (Altarelli-Parisi) evolution equations[27]—the moments of which are represented by the last line in Eq. (3.8). It should be stressed again that the $Q_0{}^2$ dependence in Eq. (3.12) or (3.8) of the (regularizing) boundary conditions remains even if one chooses vanishing input distributions, i.e., $q_i^\gamma(x,Q_0{}^2)=0$, which implies that the additive hadronic terms proportional to $q_{i,\mathrm{had}}^\gamma$ in Eq. (3.12) are absent.

The regularizing effects of the $Q_0{}^2$-dependent terms in Eq. (3.12) are demonstrated in Fig. 6 where we show the full HO solutions (solid curves) as well as the ones without the purely hadronic pieces $q_{i,\mathrm{had}}^\gamma$ in Eq. (3.12) (long-dashed curves): In contrast to the unphysical negative values of the asymptotic solution for F_2^γ at small values of x, as shown in Fig. 5 and by the short-dashed curves in Fig. 6, the general full solution is finite and perfectly *positive*.[28] The price to pay for obtaining the full solution, i.e., a physically as well as mathematically sensible result, is the so far arbitrary hadronic input $q_i^\gamma(x,Q_0{}^2)$ at an appropriately chosen value of $Q_0{}^2$. Thus at presently measured values of Q^2 it is illusory to use just the "unique" asymptotic solution for $F_2^\gamma(x,Q^2)$ as a test of QCD and as a way to determine Λ. Since the positive a_i terms in Eq. (3.12) or (3.8), become suppressed at small values of Q^2 ($\lesssim 10$ GeV^2) as compared to the negative b_i terms, the full solution turns negative in the large-x region as shown in Fig. 6 for $Q^2=3$ GeV^2. Although this large-x region lies already in the resonance region $W<2$ GeV where perturbative parton-model calculations are not applicable anymore, such negative results are *irrelevant* also since they have been obtained by using the *same* input distributions $q_i^\gamma(x,Q_0{}^2)$ as for the LO calculations. We have performed this somewhat academic calculation in order to demonstrate the magnitude of the HO contributions *per se* in Eqs. (3.4) and (3.8) or equivalently in Eq. (3.12). Within the same spirit we illustrate the dependence of the full (academic) HO solutions on Q^2 and Λ in Fig. 7.

Realistically, however, HO calculations afford in general a *different* input than the LO ones for being compared with experiment as has been discussed at the beginning of Sec. III—an analogous situation to the one encountered in deep-inelastic lepton-nucleon scattering.[20–22] Since, as in the LO case in Sec. II, present experiments are too scarce to determine the three nonperturbative input quantities $q_i^\gamma(x,Q_0{}^2)$ we have fixed this input in the following way in order to obtain more realistic HO predictions. The (small) photonic gluon distribution has been fixed by counting-rule arguments as described in Sec. II, whereas the fermionic input distributions[29] have been determined at $Q_0{}^2=1$ GeV^2 so that, when evolved to $Q^2=5.9$ GeV^2, the full HO expression for $F_2^\gamma(x,Q^2)$ in Eq. (3.12) reproduces the PLUTO data[16] at $Q^2=5.9$ GeV^2. A similar procedure for fixing the input for a LO calculation would now enable us to compare the LO results with the HO ones at different values of $Q^2>5.9$ GeV^2 with experiment. Since such measurements are not yet available[16,30] we choose, as an example, a LO input such that the final LO result for $F_2^\gamma(x,Q^2)$ coincides with

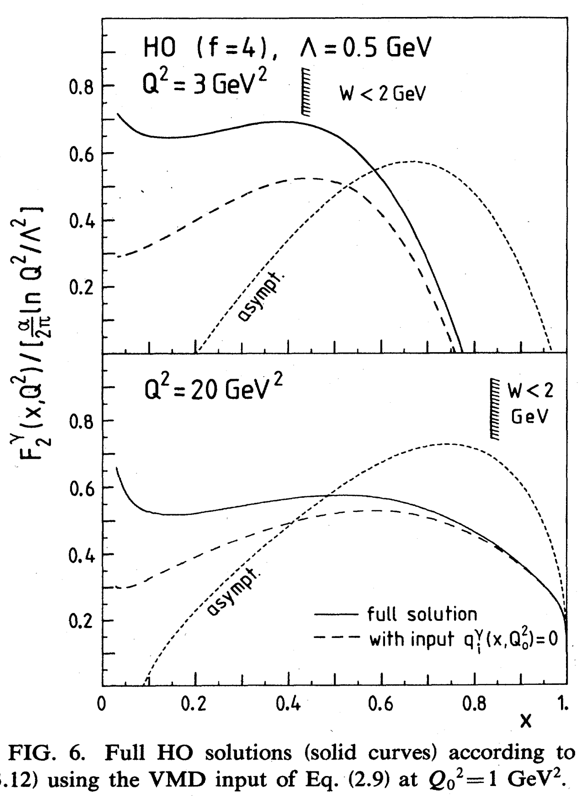

FIG. 6. Full HO solutions (solid curves) according to Eq. (3.12) using the VMD input of Eq. (2.9) at $Q_0{}^2=1$ GeV^2. The long-dashed curves show the effect of the boundary conditions for vanishing hadronic input distributions. The asymptotic solutions (short-dashed curves) are the same as the solid curves in Fig. 5. Only predictions corresponding to $W\gtrsim 2$ GeV should be considered; these lie to the left of the vertical shaded bars.

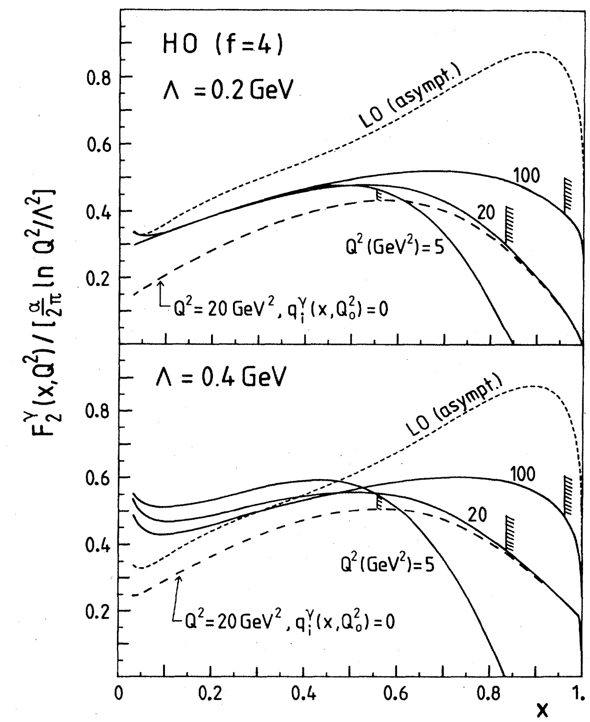

FIG. 7. Full HO predictions for $f=4$ flavors and for various values of Q^2 and Λ. The vertical shaded bars indicate, as in Fig. 6, the resonance region $W<2$ GeV. For comparison the asymptotic LO predictions are shown by the short-dashed curves which are the same as in Fig. 1. These HO results should not be compared with actual measurements since they have been obtained, as in Fig. 6, by using the same input at $Q_0{}^2$ as for the LO calculations.

the above HO prediction at $Q^2=24$ GeV^2 where the whole relevant x range lies already outside the resonance region. The differences for the predicted $F_2^\gamma(x,Q^2)$ at different values of Q^2 are now entirely due to the differences between the LO and HO *evolutions* and are shown in Fig. 8. The differences are indeed very small throughout the experimentally accessible region[16,30] and it appears unlikely that present and future experiments will become accurate enough to distinguish between the LO and HO predictions for the evolution of $F_2^\gamma(x,Q^2)$. This result is very similar to the one obtained in deep-inelastic lepton-nucleon scattering.[18,21] Had we chosen the LO input such that the resulting $F_2^\gamma(x,Q^2)$ coincides with the HO result for F_2^γ at $Q^2=5.9$ GeV^2, the predictions at $Q^2=110$ GeV^2 are only insignificantly different from the ones shown in Fig. 8.

Since LO and HO predictions for $F_2^\gamma(x,Q^2)$ are very similar throughout the presently accessible range of Q^2 (Fig. 8) and therefore indistinguishable by present experiments,[16,30] it is advantageous and easier to compare the LO predictions for $F_2^\gamma(x,Q^2)$ with experiment which are obtained from the much simpler evolution equations (2.1) and the relation (2.4). Thus we will now turn to a more detailed comparison of LO predictions with experiment, keeping in mind that the somewhat more involved HO calculations yield essentially very similar results.

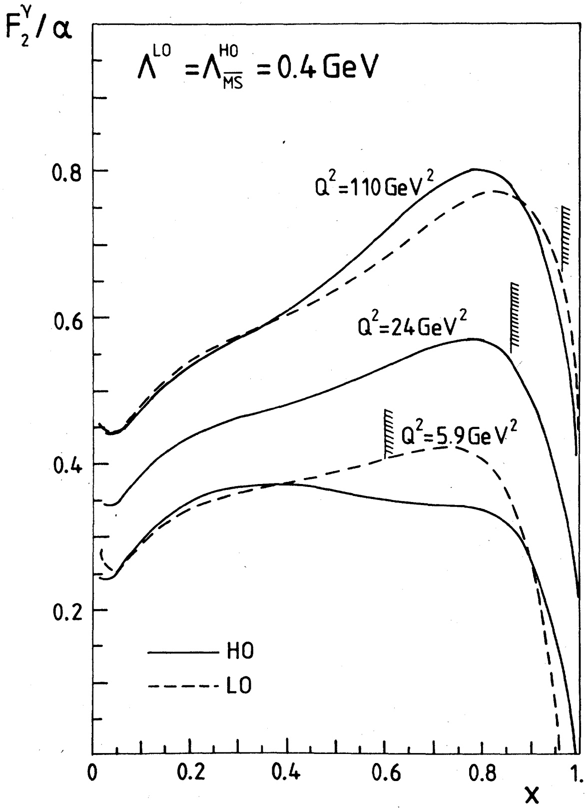

FIG. 8. Comparison of leading- and (realistic) higher-order predictions for $F_2^\gamma(x,Q^2)$. The different input distributions at $Q_0{}^2$ are described in the text and have been chosen such that the resulting LO and HO predictions for $F_2^\gamma(x,Q^2)$ coincide at $Q^2=24$ GeV^2.

C. Comparison with experiment

Since most two-photon data have not been unfolded yet,[16,30] they cannot be directly compared with QCD predictions at present. The only exceptions are the PLUTO data[16] in the range $1<Q^2<18$ GeV^2 usually referred to an average $\langle Q^2\rangle=5.9$ GeV^2 which are shown in Fig. 9 and compared with various model predictions. Usually[9,16,30] the data for F_2^γ are compared with the asymptotic LO (or HO) predictions supplemented naively by the VMD contributions in Eq. (2.9); such a prediction is denoted by LO$_{as}$ + VMD in Fig. 9: It is obvious that a better agreement with experiment for $x \lesssim 0.5$ can be easily obtained by modifying[16] the VMD contribution and/or decreasing the value of Λ. Such an agreement, however, is illusory since the hadronic $Q_0{}^2$-dependent pieces are large, causing the full solution (denoted by LO + VMD) to fall far below the data. In order to obtain a perfect

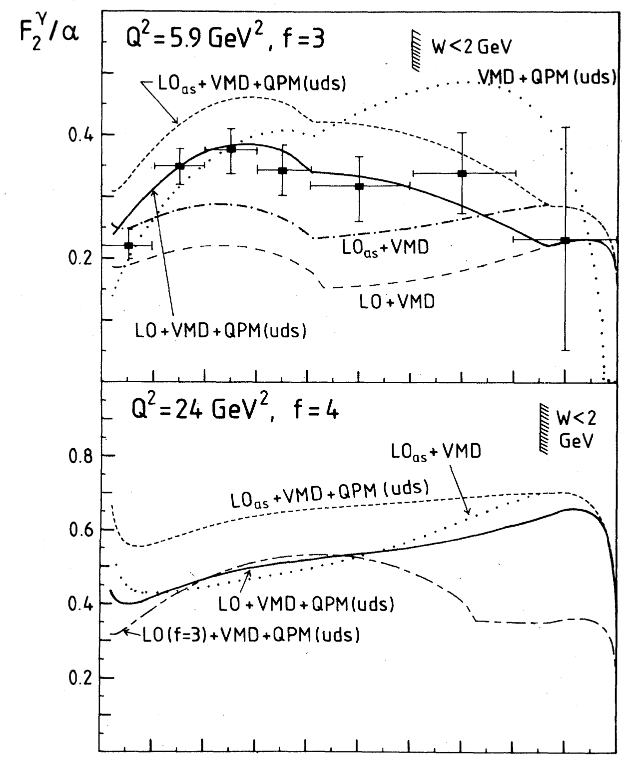

FIG. 9. Predictions for $F_2^\gamma(x,Q^2)$ at $Q^2=5.9$ and 24 GeV^2. The QCD calculations refer to $\Lambda=0.4$ GeV and the charm contributions according to Eq. (2.13) have been added to all $f=3$ results. The dotted curve at $Q^2=5.9$ GeV^2 denoted by VMD + QPM(*uds*) refers to using $q\zeta_{PM}(x,Q^2=5.9$ GeV$^2)$ as given in Eq. (3.13). For all other curves QPM was *evolved* according to the standard Altarelli-Parisi equations using $q\zeta_{PM}(x,Q^2=Q_0{}^2)$ as input at $Q_0{}^2=1$ GeV^2. The VMD is always as usual evolved from $Q_0{}^2=1$ GeV^2. The purely asymptotic predictions LO$_{as}$ refer to Eq. (2.5) whereas LO refers to our full $Q_0{}^2$-dependent solutions. The vertical shaded bars indicate the resonance region $W<2$ GeV where perturbative predictions are inappropriate. The (preliminary) PLUTO data at $\langle Q^2\rangle=5.9$ GeV^2 are taken from Ref. 16.

agreement with the PLUTO data we have therefore chosen to supplement the VMD input (2.9) at $Q_0{}^2=1$ GeV^2 by the naive quark-parton-model (QPM) box contribution for light quarks (u,d,s). This latter expression follows directly from Eq. (2.13) in the limit $4m_q{}^2/Q^2 \ll 1$ and, for a specific quark flavor, is given by[31]

$$q^{\gamma}_{\rm QPM}(x,Q^2) = 3e_q{}^2 \frac{\alpha}{2\pi}\left[8x(1-x)-1 + [x^2+(1-x)^2]\ln\left[\frac{Q^2}{m_q{}^2}\frac{1-x}{x}\right]\right], \quad (3.13)$$

where for the effective light constituent quark masses we have taken throughout

$$m_u = m_d = 0.2\ \text{GeV}, \quad m_s = 0.3\ \text{GeV}\ . \quad (3.14)$$

Although the resulting full solution, denoted by LO + VMD + QPM(uds) in Fig. 9, is in good agreement with the data it should be kept in mind that, in contrast to the asymptotic solution, this result depends strongly on the (partly) unknown or guessed hadronic inputs VMD and QPM(uds) at $Q_0{}^2=1$ GeV^2. The latter is very sensitive to the chosen values of quark masses in Eq. (3.14) and the VMD + QPM(uds) contribution to F_2^{γ} has to be larger than the perturbative QCD prediction in order to achieve this agreement with experiment. It is therefore mainly the predicted Q^2 *evolution* which can be seriously tested with present experiments once the input at a given value of Q^2 has been guessed—a situation similar to the case of deep-inelastic lepton-nucleon scattering. Thus the predictions for $Q^2=24$ GeV^2 in Fig. 9 and for $Q^2=45$ and 110 GeV^2 in Fig. 10 should provide us with further tests of QCD when compared with forthcoming unfolded data obtained by the[16,30] JADE ($Q^2=24$ and 110 GeV^2) and PLUTO ($Q^2=45$ GeV^2) collaborations. It should be noted that our evoluted results at $Q^2 > Q_0{}^2$ in Figs. 9 and 10 remain unaltered if we choose appropriate input distributions at $Q_0{}^2=5.9$ GeV^2 instead of $Q_0{}^2=1$ GeV^2.

As demonstrated above in Sec. III B, the HO predictions will differ only insignificantly from the LO ones shown in Figs. 9 and 10. Furthermore it should be kept in mind that, as soon as high-statistics data at various values of Q^2 become available, a more detailed analysis will become meaningful, in particular a model-independent determination of the thus far unknown hadronic input $q_i^{\gamma}(x,Q_0{}^2)$. Furthermore, the agreement or disagreement with experiment might even be misleading at present since the data, which refer to an *average* value of Q^2, include a wide range of measured values of Q^2. On the other hand, the theoretical predictions depend rather strongly on the specific value of Q^2. Therefore, as soon as high-statistics experiments become feasible, it should be mandatory for experimentalists to present their data at various fixed (and not averaged) values of Q^2 in order to allow for a clean comparison with theoretical predictions. In Figs. 9 and 10 the vertical shaded bars indicate the region where the invariant 2γ energy W becomes smaller than 2 GeV, thus entering the resonance region. Therefore the pointlike and perturbative parton calculations should *not* be taken seriously in large-x regions where $W<2$ GeV.

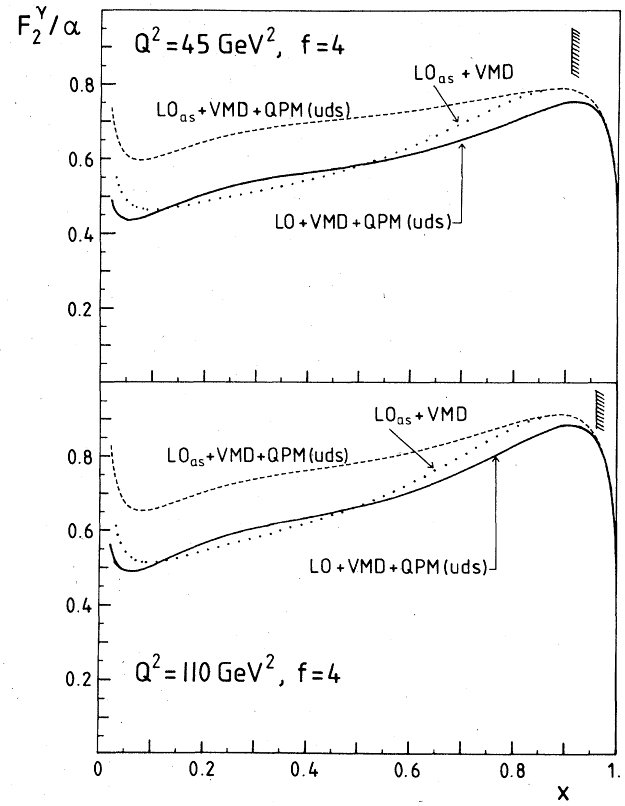

FIG. 10. Predictions for $F_2^{\gamma}(x,Q^2)$ at $Q^2=45$ and 110 GeV^2 using $\Lambda=0.4$ GeV. The notations are as in Fig. 9.

At small values of Q^2, where $Q^2 \not\gg 4m_c{}^2$, charm is not fully excited yet and one has to use the lowest-order Bethe-Heitler expression (2.13) to account for charm production. Thus only the $f=3$ flavor QCD predictions are relevant in this region and *not* the resummed (evolved) $f=4$ results. These results are shown in Fig. 9 for $Q^2=5.9$ GeV^2 and, although not explicitly stated, all $f=3$ predictions are always supplemented by $F^{\gamma}_{2,c}$ of Eq. (2.13). For intermediate values of Q^2 the truth lies somewhere between these $f=3$ predictions and the $f=4$ results: Therefore in Fig. 9 we show for $Q^2=24$ GeV^2 some predictions for $f=3$ flavors as well. For large values of Q^2($\gtrsim 50$ GeV^2) the $f=4$ flavor results, shown in Fig. 10, should already be adequate. It might be interesting to mention that for such large values of Q^2 the $f=3$ [supplemented by Eq. (2.13)] and the $f=4$ results differ by less than 10% as long as $x \lesssim 0.7$.

Finally in Fig. 9 we show also the "prediction" of just the naive QPM box for light quarks at $Q^2=5.9$ GeV^2, supplemented by VMD and charm production [Eq. (2.13)], which is denoted by VMD + QPM(uds). The use of the naive box expression (3.13) at $Q^2=Q_0{}^2 \simeq 1$ GeV^2 together with Eq. (3.14) for the effective constituent quark masses is certainly within the realm of our present understanding of constituent quark masses.[32,33] However, at larger values of Q^2 the use of Eq. (3.13) together with quark masses as large as in Eq. (3.14) is doubtful, to say

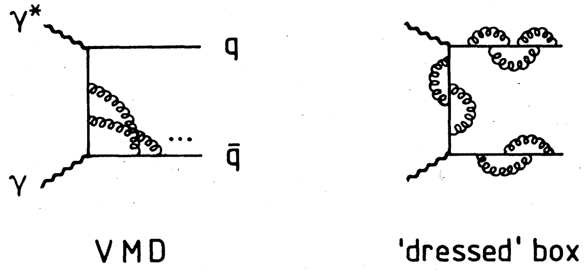

FIG. 11. Nonperturbative VMD diagram and the "dressed" box giving rise to Q^2-dependent quark masses as in Eq. (3.15).

the least, and certainly lacks any theoretical basis. This is so because constituent or "soft" masses fall off[32] with Q^2,

$$m_q(Q^2) \sim g_s^{\,2}(Q^2)\frac{\langle \bar{q}q \rangle}{Q^2} \tag{3.15}$$

for momenta large compared to the chiral-symmetry-breaking scale, where the soft mass is produced by chiral symmetry breaking ($\langle \bar{q}q \rangle \neq 0$). On the basis of an effective QCD Lagrangian it has been recently concluded[33] that this chiral-symmetry-breaking scale should in turn be of the order of about 1 GeV, below which nonperturbative effects become relevant.[33] This gives us, besides the experimental indications,[11] further confidence in our choice for the (hadronic) input variable $Q_0^{\,2} \simeq 1$ GeV^2, to be interpreted as the chiral-symmetry-breaking scale. Thus $q^{\gamma}_{\mathrm{QPM}}$ in Eq. (3.13) should always be viewed in connection with Eq. (3.15) as a result[32] of the fully "dressed" box illustrated in Fig. 11; quark masses quickly reduce to their current mass values ($m_u \simeq 4$ MeV, $m_d \simeq 7$ MeV, $m_s \simeq 150$ MeV) when Q^2 becomes larger than 1 GeV^2. Therefore a comparison[9,16] of $q^{\gamma}_{\mathrm{QPM}}(x,Q^2)$ in Eq. (3.13) with experiments at *large* values of Q^2 using (constant) quark masses as large as in Eq. (3.14) is rather meaningless within the framework of QCD.[32,33]

To enable a comparison with other future experiments we present more detailed predictions in Figs. 12 and 13 for the VMD and QPM inputs of Eqs. (2.9) and (3.13), respectively, taken at $Q_0^{\,2}=1$ GeV^2 which yielded the best agreement with present PLUTO data at $Q^2=5.9$ GeV^2 in Fig. 9.

Finally, in Fig. 14 we compare, at a fixed value of $x=0.4$, the predicted Q^2 dependences of LO and HO calculations using different inputs at $Q_0^{\,2}=1$ GeV^2 as in Fig. 9. Although the absolute normalization depends critically on the hadronic input chosen (or fitted) at $Q_0^{\,2}$, the increase with $\ln Q^2/\Lambda^2$ for $Q^2 \gtrsim 10$ GeV^2, typically predicted by QCD, is rather insensitive to this input. For deep-inelastic photon-photon scattering it therefore appears that the only clean test of QCD, which is independent of

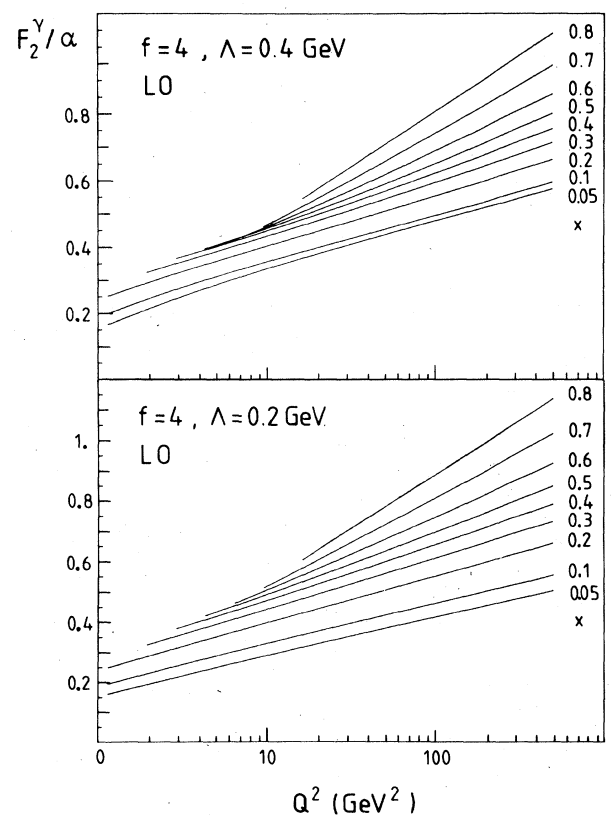

FIG. 12. Full leading-order predictions for the Q^2 dependence of $F_2^\gamma(x,Q^2)$ for fixed values of x using the VMD in Eq. (2.9) *and* the light (u,d,s) QPM box of Eq. (3.13) as input at $Q^2=Q_0^{\,2}=1$ GeV^2.

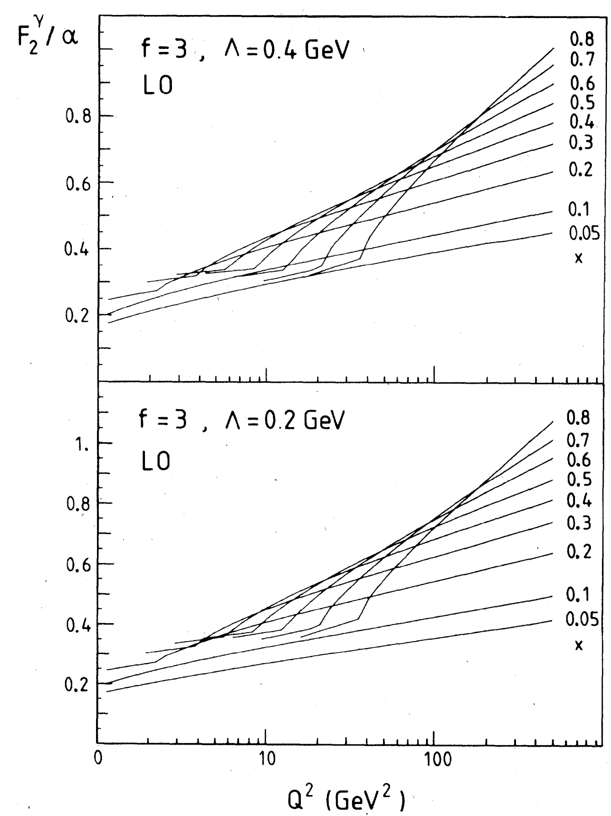

FIG. 13. Same predictions as in Fig. 12 but for $f=3$; charm contributions have been added according to Eq. (2.13).

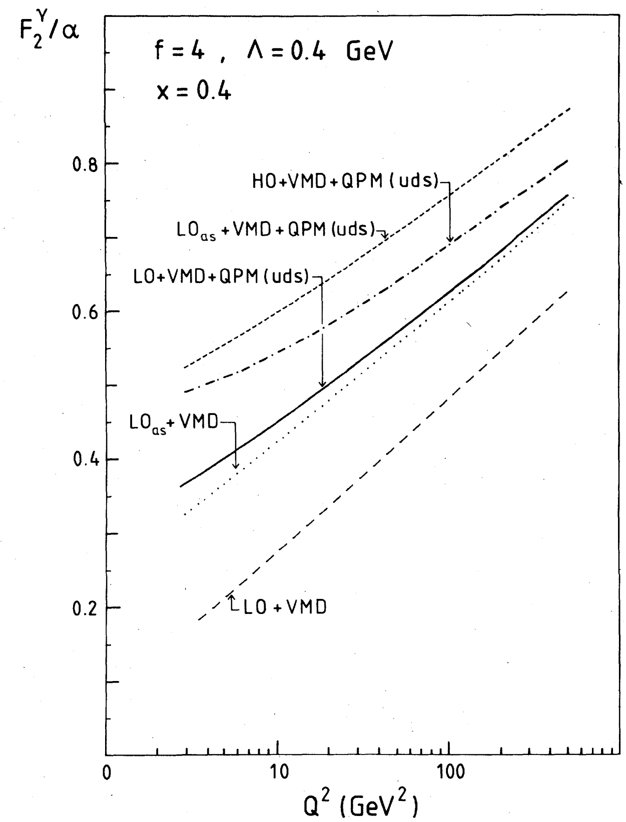

FIG. 14. Comparison of the predicted Q^2 dependences of various LO and HO calculations at a fixed value of $x=0.4$. The notations and inputs are as in Fig. 9. The input distributions for the HO result have been chosen to be the same as the ones for the LO calculations described in Fig. 9.

the ill-understood hadronic input, is the observation of an increase of $F_2^\gamma(x,Q^2)$ with $\ln Q^2/\Lambda^2$ for fixed values of x.

IV. CONCLUSIONS

We have argued that there are two representations for the general solution of the photon evolution equations. These are the traditional solution,[1,2] consisting of a "pointlike" part plus a *regular* hadronic (VMD) input, and the one of Ref. 3 referred to as the "full solution." The pointlike (asymptotic) part of the traditional solution is *singular* in the leading order[1] and also in the higher order[2] with a *negative* singularity.[4] Together with its *regular* hadronic input it thus yields a *singular*, even negative at HO, structure function. One can obviously improve this shortcoming of the traditional solution by taking a *singular* hadronic input which compensates[5] the singularities of the pointlike component. This, however, then amounts to our full solution.

The comparison of the singular traditional solution with the data is meaningless and wrong. There is no value of Q^2, however large, where it is "safe" even in the intermediate-x region.[10] The realization that the hadronic input should always play a crucial role via the boundary conditions of our regular solution leads to the disappointing conclusion that there are, in fact, *no* "absolute predictions" (i.e., only Λ-dependent predictions) for the photon structure function. The effects of choosing $Q_0^2 \simeq 1$ GeV^2 are *significant even in regions of Q^2 and x where our hadronic input function is already negligible.* This holds for all presently available or foreseeable values of Q^2. Thus the usual extraction of Λ from the pointlike asymptotic solution,[1,2] combined with a regular hadronic input, is no more than a very unreliable *guess*. It could be correct by some fortunate accident but the reliable determination of Λ affords a careful assessment of the hadronic input functions. These afford *measurements* of $F_2^\gamma(x,Q^2)$ at various values of Q^2. The value of Λ can then be determined from the QCD-predicted and Λ-dependent evolution of $F_2^\gamma(x,Q^2)$ as compared to experimental measurements at higher values of Q^2. The situation is thus exactly the same as already encountered for the nucleon structure functions. Only the observation of a linear increase with $\ln Q^2/\Lambda^2$ of F_2^γ at fixed values of x would provide us with a clean test of QCD—a prediction which is rather insensitive to the hadronic input at Q_0^2.

After these general remarks, let us turn to somewhat more concrete conclusive remarks and summary of our results:

(i) One should not consider the resonance region

$$x > x_{\max} = Q^2/(Q^2 + W_{\min}^2)\ ,$$

where $W_{\min} \simeq 2$ GeV, in comparing with the data.

(ii) The hadronic inputs $q_i^\gamma(x,Q_0^2)$, should be *separately* determined for the LO and the HO analysis of future high-statistics data since they can obviously be *different*—in analogy to deep-inelastic lepton-nucleon scattering.[20–22]

(iii) For $Q^2 \lesssim 20$ GeV^2 do *not* use full $f=4$ flavor QCD results, but instead $f=3$ flavor results supplemented by lowest-order QPM (Bethe-Heitler) for charm production. For $Q^2 \gtrsim 50$ GeV^2 the $f=4$ predictions are presumably already adequate.

(iv) Theoretical calculations should be performed *directly* in x space. Fitting to integer-n moments is too inaccurate.

(v) Future data should *not* be averaged over Q^2 since QCD predicts a rather strong Q^2 dependence of $F_2^\gamma(x,Q^2)$. Averaged Q^2 data, $F_2^\gamma(x,\langle Q^2\rangle)$, are thus not very useful and might even be misleading when compared to QCD.

(vi) It is seen from Fig. 9 that in LO the hadronic input VMD + QPM(*uds*) at $Q_0^2=1$ GeV^2 combined with standard values of Λ reproduces the data at $\langle Q^2\rangle = 5.9$ GeV^2. Furthermore it should be noticed that for values of Q^2 as low as 5.9 GeV^2 one *cannot* convincingly test the pointlike structure of the photon dominating in the *large-x* region: The constraint $W \gtrsim 2$ GeV abolishes the interesting region $x > 0.6$.

(vii) In the physically relevant x region ($W \gtrsim 2$ GeV, i.e., $x < x_{\max}$) the difference between HO and LO *predictions* is small and perturbative calculations are thus reliable. Present experiments are far too inaccurate to distinguish between these LO and HO predictions as in the corresponding case of deep-inelastic lepton-nucleon scattering.[18,21]

(viii) Predictions for forthcoming experiments at $Q^2=24$, 45, and 110 GeV^2 for various hadronic inputs are given in Figs. 9 and 10, and further detailed predictions can be found in Figs. 12 and 13 using a VMD + QPM(uds) input at $Q_0{}^2=1\ \mathrm{GeV}^2$.

Note added. While completing the manuscript we received a very recent paper from G. Rossi [Phys. Rev. D **29**, 852 (1984)], which is essentially a shorter version of his paper cited in Ref. 25 and where in addition the $Q_0{}^2$-dependent input boundary conditions for a *real-photon* target have been included and discussed as suggested in Ref. 3.

ACKNOWLEDGMENTS

We thank H. Spitzer for helpful conversations and advice concerning experimental questions and problems; furthermore we are indebted to Ch. Berger for remarks on presently available deep-inelastic photon-photon data. We would also like to thank M. Drees for discussions and in particular for his collaboration in calculating LO and HO predictions using appropriate different input distributions.

---

[1]E. Witten, Nucl. Phys. **B120**, 189 (1977).

[2]W. A. Bardeen and A. J. Buras, Phys. Rev. D **20**, 166 (1979); **21**, 2041(E) (1980).

[3]M. Glück and E. Reya, Phys. Rev. D **28**, 2749 (1983); more detailed quantitative results including the effects of the $Q_0{}^2$ dependent input boundary conditions, calculated directly in x space, have been presented by M. Glück, in *Proceedings of the International Europhysics Conference on High Energy Physics, Brighton, 1983,* edited by J. Guy and C. Costain (Rutherford Appleton Laboratory, Chilton, Didcot, United Kingdom, 1984), p. 180.

[4]D. W. Duke and J. F. Owens, Phys. Rev. D **22**, 2280 (1980).

[5]W. A. Bardeen, in *Proceedings of the 1981 International Symposium on Lepton and Photon Interactions at High Energies, Bonn,* edited by W. Pfeil (Physikalisches Institut, Universität Bonn, Bonn, 1981), p. 432.

[6]R. J. DeWitt, L. M. Jones, J. D. Sullivan, D. E. Willen, and H. W. Wyld, Jr., Phys. Rev. D **19**, 2046 (1979).

[7]W. R. Frazer and J. F. Gunion, Phys. Rev. D **20**, 147 (1979).

[8]In order to obtain a rapid convergence for the iterative solutions of leading- and higher-order evolution equations we have used the convergence factor suggested in Ref. 6.

[9]W. R. Frazer, in *Proceedings of the Vth International Conference on Two-Photon Physics, Aachen, 1983,* edited by Ch. Berger (Springer, New York, 1984), p. 377.

[10]G. Rossi, Phys. Lett. **130B**, 105 (1983).

[11]For recent reviews see, for example, in *Physics in Collision: High Energy ee/ep/pp Interactions,* proceedings of the 2nd International Conference, Stockholm, 1982, edited by P. Carlson and W. P. Trower (Plenum, New York, 1983); D. Cords, in *Physics at Very High Energies,* proceedings of the SLAC Summer Institute on Particle Physics, 1982, edited by Anne Mosher (SLAC Report No. 259, 1983).

[12]J. Busenitz and J. D. Sullivan, Phys. Rev. D **24**, 1794 (1981).

[13]J. F. Owens and E. Reya, Phys. Rev. D **17**, 3003 (1978).

[14]Here we disagree with the statements of C. Peterson, P. M. Zerwas, and T. F. Walsh, Nucl. Phys. **B229**, 301 (1983).

[15]E. Witten, Nucl. Phys. **B104**, 445 (1976); M. Glück and E. Reya, Phys. Lett. **83B**, 98 (1979).

[16]Ch. Berger, in *Proceedings of the 1983 International Symposium on Lepton and Photon Interactions at High Energies, Ithaca, New York,* edited by D. G. Cassel and D. L. Kreinick (Cornell University, Ithaca, 1984).

[17]It should be noted that $k_G^{(1)}(x)$ includes a Dirac δ function $\delta(1-x)$. The following appropriate representation for the δ function has been adopted for our numerical calculations:

$$\delta(1-x)=\frac{2}{\epsilon\sqrt{\pi}}\exp[-(1-x)^2/\epsilon^2]$$

with $\epsilon=5\times10^{-4}$.

[18]E. Hoffmann and E. Reya, Phys. Rev. D **27**, 2630 (1983).

[19]M. Glück and E. Reya, Phys. Rev. D **25**, 1211 (1982).

[20]L. Baulieu and C. Kounnas, Nucl. Phys. **B141**, 423 (1978); J. Kodaira and T. Uematsu, *ibid.* **B141**, 497 (1978).

[21]G. Altarelli, R. K. Ellis, and G. Martinelli, Nucl. Phys. **B143**, 521 (1978); **B146**, 544(E) (1978); A. Bialas and A. J. Buras, Phys. Rev. D **21**, 1825 (1980).

[22]For comprehensive reviews on this subject, see A. J. Buras, Rev. Mod. Phys. **52**, 199 (1980); A. Peterman, Phys. Rep. **53**, 157 (1979).

[23]In order to achieve a rapid convergence we have chosen initial inputs for the iteration functions which have already the correct behavior for $x\to1$. These can be obtained by extracting the dominant contributions from the convolution on the LHS of Eq. (3.1) for $x\to1$ using

$$\int_x^1\frac{dy}{(1-y)_+}b_i\left[\frac{x}{y}\right]\simeq-b_i(x)\int_0^x\frac{dy}{1-y}\ .$$

This yields

$$b_{\mathrm{NS},\Sigma}(x)=-\frac{A_{\mathrm{NS},\Sigma}(x)}{\frac{8}{3}\ln(1-x)+2-c}\ ,$$

$$b_G(x)=-\frac{A_G(x)}{6\ln(1-x)+11/12-f/18-c}\ ,$$

as zeroth input for the iteration and $A_i(x)$ denotes the RHS of Eq. (3.6); furthermore we have added an arbitrary constant c to the nominator and denominator which has been taken to be $c=10$ in order to avoid the vanishing of the denominator in the x range considered. Other input choices yield the same final results but with less rapid convergence.

[24]The situation here is similar to the case of deep-inelastic lepton-hadron scattering (see, for example, Ref. 18); for a recent general discussion we refer the reader to Ref. 19 and references therein. It should, however, be emphasized that the unwanted contributions of the $O(\alpha_s)$ terms are more serious in two-photon physics because of the inhomogeneous Born terms k_i in the evolution equations (3.1) which prevent the photon structure function from being power suppressed in $(1-x)$ as $x\to1$.

[25]Such a regularization has already been observed for the case of a *massive* target phonon, i.e., for *virtual-photon* structure

functions where also the second photon in $\gamma(Q^2)\gamma(-p^2) \to$ hadrons is off shell, i.e., $-p^2 \gtrsim 1$ GeV$^2 \gg \Lambda^2$: T. Uematsu and T. F. Walsh, Nucl. Phys. **B199**, 93 (1982); G. Rossi, Ph.D. thesis, University of California, San Diego, Report No. UCSD-10P10-227, 1983.

[26]D. J. Gross, Phys. Rev. Lett. **32**, 1071 (1974); G. Parisi, Phys. Lett. **50B**, 367 (1974).

[27]Actual calculations show that the standard HO QCD evolutions of the hadronic input distributions differ marginally (at most 10%) from those in LO. Since the latter calculations are far less time consuming we have chosen to evolute $q_i^\gamma(x,Q_0^2)$ with the LO equations and added the result to $F_2^\gamma(x,Q^2)$ according to Eq. (2.4) instead of the last three hadronic terms in Eq. (3.12). In view of the rather uncertain input $q_i^\gamma(x,Q_0^2)$ at present, such an approximation is perfectly legitimate.

[28]All calculations are performed in the $\overline{\rm MS}$ scheme. The results using the MOM scheme are practically the same.

[29]Lacking any further experimental information we have to make a further assumption about the input distributions at Q_0^2 in order to extract them from one measured structure function[16] $F_2^\gamma(x,Q^2)$ at $Q^2=5.9$ GeV^2. Neglecting the small sea part of Σ^γ we choose, for example,

$$\Sigma^\gamma(x,Q^2)=\frac{\langle e^2\rangle}{\langle e^4\rangle-\langle e^2\rangle^2}\, q_{\rm NS}^\gamma(x,Q^2)$$

which by experience is expected to hold to within 5% for $x \gtrsim 0.1$. Different choices for the inputs Σ^γ and $q_{\rm NS}^\gamma$ do not change our conclusions. The PLUTO data (Ref. 16) at $Q^2=5.9$ GeV^2 are then well represented by Eq. (3.12) with the HO input chosen at $Q_0^2=1$ GeV^2 as

$$q_{\rm NS}^\gamma(x,Q_0^2)=15x^9\ln^{-2}(1-x)+4(1-x)^4\ .$$

We have explicitly checked that fixing $q_{\rm NS}^\gamma(x,Q_0^2)$ at any other (larger) value of Q_0^2 such as always to reproduce the PLUTO data, our evoluted results at arbitrary values of Q^2 remain practically unaltered. More details will be presented in a forthcoming publication by M. Drees, M. Glück, K. Grassie, and E. Reya.

[30]H. Spitzer, in *Proceedings of the Vth International Conference on Two-Photon Collisions, Aachen, 1983* (Ref. 9), p. 318.

[31]Since

$$F_{2,{\rm QPM}}^\gamma=2x\sum_{q=u,d,s} e_q^2 q_{\rm PM}^\gamma(x,Q^2)\ ,$$

it is straightforward to obtain the required nonsinglet and singlet input distributions at $Q^2=Q_0^2$ as in Eq. (2.9):

$$q_{\rm NS,QPM}^\gamma(x,Q_0^2)=2(\tfrac{2}{9}u_{\rm PM}^\gamma-\tfrac{1}{9}d_{\rm PM}^\gamma-\tfrac{1}{9}s_{\rm PM}^\gamma)\ ,$$

$$\Sigma_{\rm PM}^\gamma(x,Q_0^2)=2(u_{\rm PM}^\gamma+d_{\rm PM}^\gamma+s_{\rm PM}^\gamma)\ .$$

[32]H. D. Politzer, Nucl. Phys. **B117**, 397 (1976).

[33]A. Manohar and H. Georgi, Nucl. Phys. **B234**, 189 (1984).